Published in final edited form as:
Aging Cell. 2012 October ; 11(5): 741–750. doi:10.1111/j.1474-9726.2012.00840.x.

Temporal analysis of vascular smooth muscle cell elasticity and adhesion reveals oscillation waveforms that differ with aging

Yi Zhu[1,2], **Hongyu Qiu**[2], **Jerome P. Trzeciakowski**[3], **Zhe Sun**[1], **Zhaohui Li**[1], **Zhongkui Hong**[1], **Michael A. Hill**[1], **William C. Hunter**[2,4], **Dorothy E. Vatner**[2], **Stephen F. Vatner**[2], and **Gerald A. Meininger**[1]

[1]Dalton Cardiovascular Res Center and Department of Medical Pharmacology and Physiology, Univ of Missouri, Columbia, MO.

[2]Department of Cell Biology and Molecular Medicine, UMDNJ-New Jersey Med School, Newark, NJ.

[3]Department of Systems Biology and Translational Medicine, Texas A&M University, College Station, TX.

[4]Department of Biomedical Engineering, New Jersey Institute of Technology, Newark, NJ.

Abstract

A spectral analysis approach was developed for detailed study of time-resolved, dynamic changes in vascular smooth muscle cell (VSMC) elasticity and adhesion to identify differences in VSMC from young and aged monkeys. Atomic force microscopy (AFM) was used to measure Young's modulus of elasticity and adhesion as assessed by fibronectin (FN) or anti-beta 1 integrin interaction with the VSMC surface. Measurements demonstrated that VSMC cells from old versus young monkeys had elevated elasticity (21.6 kPa vs 3.5 kPa or a 612% elevation in elastic modulus) and adhesion (86 pN vs 43 pN or a 200% increase in unbinding force). Spectral analysis identified three major frequency components in the temporal oscillation patterns for elasticity (ranging from 1.7×10^{-3} to 1.9×10^{-2} Hz in old and 8.4×10^{-4} to 1.5×10^{-2} in young) and showed that the amplitude of oscillation was larger ($p<0.05$) in old than in young at all frequencies. It was also observed that patterns of oscillation in the adhesion data were similar to the elasticity waveforms. Cell stiffness was reduced and the oscillations were inhibited by treatment with cytochalasin D, ML7 or blebbistatin indicating involvement of actin-myosin driven processes. In conclusion, these data demonstrate the efficacy of time-resolved analysis of AFM cell elasticity and adhesion measurements and that it provides a uniquely sensitive method to detect real-time functional differences in biomechanical and adhesive properties of cells. The oscillatory behavior suggests mechanisms governing elasticity and adhesion are coupled and affected differentially during aging which may link these events to changes in vascular stiffness.

Corresponding Authors (shared senior authors): Gerald A. Meininger, Ph.D., Director, Dalton Cardiovascular Research Center, Margaret Proctor Mulligan Professor in Medical Research, Department of Medical Pharmacology and Physiology, University of Missouri-Columbia, 134 Research Park Drive, Columbia, MO 65211, USA Phone: 573-882-9662 Fax: 573-884-4232 Meiningerg@missouri.edu and Stephen F. Vatner, MD, Department of Cell Biology, UMDNJ, New Jersey Medical School, 185 South Orange Ave, Newark, NJ 07103 vatnersf@umdnj.edu.

Supporting Information:
Detailed methods of Vascular smooth muscle cell isolation and cell culture, AFM contact mode imaging, elasticity and adhesion force measurement, Data processing and analysis of cell elasticity and adhesion force. Additional results that supplement the "Real time elasticity measurements in single VSMC measured by AFM" and "Real time measurement of ECM protein-integrin adhesion by AFM". Supplemental figures: Mathematical decomposition of the elastic modulus waveform for old and young VSMC treated with cytochalasin D (**Figure S1),** ML7 **(Figure S2)** or blebbistatin **(Figure S3).**

Keywords

Fibronectin; integrins; vascular smooth muscle cell contractile function; Young's modulus; cytoskeleton; mechanotransduction; extracellular matrix adhesion; force measurement; atomic force microscopy

Introduction

Mechanical forces and tissue mechanical properties play important roles in cardiovascular diseases including hypertension, stroke, aneurysms, atherosclerosis and heart disease. With increasing age, there is a well-documented elevation in vascular stiffness that has become accepted as a risk factor associated with these diseases (1-3). Reduced flexibility of the blood vessel wall has predominantly been believed to be associated with changes in the vascular extracellular matrix (ECM). In this regard, increased collagen content and decreased elastin have been identified as the most significantly altered ECM components (2,4,5). In addition to the ECM, vascular smooth muscle cells (VSMC) represent the main cellular constituents of the arterial wall and their active contractile properties provide for the active stress present within the wall. Most prior work on the mechanics of the aorta in aging has focused on the intact vessel whereas our focus on the mechanical properties of isolated VSMC has provided unique insight. In this regard, recent work from our laboratories demonstrated that VSMC isolated from aged monkeys have an elastic modulus that is approximately 3 times greater than that observed younger cells. In addition, old monkey VSMC contained more actin and had elevated integrin expression (6). This work supports the idea that VSMC may play an important role in contributing to the differences in stiffness of the vascular wall seen with aging (6). The mechanism underlying the increased cell elasticity appeared to be related to the higher actin and beta 1 integrin expression. In this regard, an actin depolymerizing agent, cytochalasin D, and the myosin light chain kinase inhibitor, ML7, both abolished the differences in elasticity (6).

The dynamic nature of the cellular cytoskeleton and cellular adhesion are well-known phenomenon in cellular biology (7,8). In VSMC cytoskeletal behavior includes contractile filament interactions involving cross-bridge cycling (9,10) and remodeling of cytoskeletal elements secondary to or in parallel with contractile activation and exposure to mechanical forces (9,10). This behavior reflects cytoskeletal functions that are both adaptive as well as dynamic in support of the contractile functions of VSMC. Together then, the time-dependent state of these properties defines the elasticity of the VSMC. Furthermore, it is well known that the cytoskeleton is physically and functionally coupled to cell adhesion (11). Through adhesions, cells exert control upon ECM assembly composition and structure (12,13). Thus, changes in adhesive behavior could be importantly linked to the ECM stiffening noted in aging. By way of adhesion to the ECM, cells also sense the rigidity of the ECM that in turn alters the signaling state of the cell (14,15). This dynamic two-way interplay between ECM adhesion and cytoskeletal properties complicates efforts to examine the properties of either component independently of the other's influence. A primary purpose of this study was, therefore, to gain insight into the differences observed between VSMC from aged and young animals by devising an analytical approach that would allow the dynamic properties of elasticity and adhesion to be characterized. To accomplish this we used an atomic force microscope (AFM), its high-sensitivity for measuring and applying pico-Newton forces to cells make it an ideal tool to characterize the mechanical and adhesive properties of single cells (20).

In this study, we undertook a more detailed investigation at the cellular level of the real-time dynamic mechanical behavior of single VSMC by developing a spectral analysis approach

that we applied to real-time measurements of VSMC elasticity and adhesion. We used this approach to compare VSMC isolated from old and young monkeys to test the hypothesis that the alterations in expression of actin and beta 1 integrin would be further evident in differences in the dynamic behavior of both the actin cytoskeleton and adhesion to a beta 1 integrin binding ECM protein.

Materials and Methods

Vascular smooth muscle cell isolation and cell culture

Vascular smooth muscle cells (VSMCs) for these studies were isolated from thoracic aorta (TA) of aged (24-25 years) and young (5-8 years) male monkeys (*Macaca fascicularis*) representing old and young groups, respectively. The male monkeys were raised and maintained according to the *Guide for the Care and Use of Laboratory Animals* (NIH 83-23, revised 1996) in the Philippines. VSMCs were isolated in the Philippines from the thoracic aorta from which the external fat, connective tissue, adventitia and endothelial layer were removed. Using immunofluorescence techniques, the phenotype of the VSMCs was confirmed by the presence of alpha-smooth muscle actin (6).

AFM contact mode imaging, elasticity and adhesion force measurement

A Bioscope System (model IVa, Veeco Mertrology Inc., Santa Barbara, CA) AFM that was mounted on an Olympus IX81 microscope (Olympus Inc., NY) was used in contact mode operation for imaging and dynamic measurements of cell elasticity and adhesion on single VSMC. AFM probes were composed of silicon nitride microlevers (model MLCT: spring constant ranging 10-30 pN/nm) and were purchased from Veeco Mertrology Inc. (Santa Barbara, CA). For adhesion measurements, experiments were conducted with AFM probes that were functionalized with fibronectin (FN) as an extracellular matrix (ECM) protein or with a beta 1 integrin antibody (HM,,1-1, Pharmingen). The probe spring constants were assumed to be unchanged after the coating process based on previous work in our laboratory (27). Probes were calibrated using the thermal noise method. The AFM system was configured so that the probes repeatedly approached and retracted from the same surface site of single VSMC surface at a frequency of 0.5Hz (tip speed 800nm/s). Force curves were continuously collected at 28-30 force curves/min for a 30 min period at room temperature in serum free media. Approach curves were used for analysis of cell contact height and cell elasticity and retraction curves were used for analysis of cell adhesion. Analysis and processing of the approach and retraction curves (512 points per curve) was automated by using our proprietary NforceR software package and Matlab (6,27).

To quantify the elasticity (Young's modulus) of VSMC, a Hertz-based model as modified by Sneddon for a rigid cone indenting a soft surface was applied to the force-indentation profile derived from the recorded approach force curve. The equation for calculation of the elastic modulus was:

$$F = \frac{2E\delta^2}{\pi(1-\upsilon^2)}\tan(\alpha)$$

where indentation force (F) was calculated by using Hooke's law ($F = \kappa\Delta x$), where κ and Δx denote the AFM probe's spring constant and the probe's measured deflection, respectively. The indentation depth (δ) is calculated fromthe difference in the *z*-movement of the AFM piezo and the deflection of the probe. E is the elastic modulus of cell being studied, and ν denotes the Poisson ratio (0.5 for cell). α represents the shape of the probe (MLCT, Veeco

Mertrology Inc., Santa Barbara, CA) that was considered to be conical with an approximated half-angle of 21.25 degrees in this report (27,31).

To test for the involvement of the actin cytoskeleton as a determinant of VSMC elasticity was measured in cells from old and young monkeys that were treated with an actin depolymerizing agent (cytochalasin D, 10 μM; Sigma, St. Louis, MO), a myosin light chain kinase inhibitor (ML7, 10 μM; Sigma, St. Louis, MO) or a myosin II inhibitor (blebbistatin, 20 μM; EMD Millipore, Billerica, MA). Following drug addition, cell elasticity was continuously measured for at least 40 min to obtain a steady-state response.

Data processing and analysis of cell elasticity and adhesion force

A spectral analysis procedure was developed for analysis and subsequent interpretation of the oscillation waveforms observed in the elasticity and force data. Eigenvalue decomposition (singular spectrum analysis; (32,33) was used to isolate three primary oscillatory components for each time-series data set. Linear trends were estimated and subtracted from each series prior to spectral analysis. To visualize the average group behavior of the oscillations, we obtained three values of amplitude, frequency and phase for every experimental subject. These individual values were then averaged: phases (φ) as a simple mean; frequencies (f) were converted to periods ($1/f$) prior to averaging; amplitudes (A) were log10-tranformed before computing the mean. The mean period and mean log-amplitude were then converted back to frequency and amplitude. A composite time series for each treatment set was constructed as:

$$y(t) = \bar{A}_1 Sin\left(2\pi \bar{f}_1 t + \bar{\phi}_1\right) + \bar{A}_2 Sin\left(2\pi \bar{f}_2 t + \bar{\phi}_2\right) + \bar{A}_3 Sin\left(2\pi \bar{f}_3 t + \bar{\phi}_3\right) + \bar{b}_1 t + \bar{b}_0$$

where b_1 and b_0 represent the slope and intercept of the linear trend, respectively, and the bar above each component indicates the average value. For comparing reconstructed signals across various data types (elasticity, unbinding force, etc.), we also repeated the spectral analysis after standardizing each time series to a mean of zero and standard deviation of 1. Standardization only affected the relative sizes of each amplitude component: frequency and phase of each component were unaffected.

From the rate of retraction and the distance along the retraction curve at which a rupture event occurred, the time of rupture could then be estimated and incorporated into a time sequence. A constraint, however, is that either a lack of adhesions or multiple adhesions during a single retraction cycle can result in unequal sampling intervals. As nearly all signal analysis algorithms are based on regular constant sampling intervals we first resampled the data by a factor of 10 using the resample function from the MATLAB Signal Processing Toolbox (release 2008b, The Math Works, Inc., Natick MA). This algorithm performs an interpolation by designing and applying an anti-aliasing low pass finite impulse response filter followed by a change in rate. After application of the resample function the interpolated data were then down-sampled to 0.5 Hz. To ensure equivalence, all measured time series (force, elasticity, contact point, displacement) were subjected to the same processing, even if the time points occurred at regular intervals (e.g. elasticity).

Statistical analysis

Data are presented as mean and S.E.M. Statistical comparisons used an unpaired two-tailed Student's t test for testing the elasticity and adhesion force differences with $p < 0.05$ considered statistically significant. For comparisons of oscillatory frequencies, amplitudes and periods, data were analyzed using multifactor ANOVA. Analyses of frequencies and amplitudes were based on the transformed values (i.e. periods and log-amplitudes). For

comparison, elasticity changes following drug treatments were analyzed using Students t-test and are displayed relative to control, pre-drug responses. Differences between selected pairs of means were tested for significance with single-degree of freedom contrasts. Differences were considered statistically significant at $p<0.05$. In Table 1, average frequencies and amplitude are listed as 1/(mean period) and antilog (mean amplitude). Standard errors of the mean frequency or mean amplitude are estimated from confidence intervals that were computed around the mean periods and mean log-amplitudes and then reverse transformed to frequency and amplitude. Probabilities related to adhesion were determined from the retraction curves and were quantified based on the fraction of curves showing 0, 1, 2, 3, or 4 adhesion events per curve. Biological variability was evaluated by computing separate probability scores for data from each monkey, then averaging. Standard 2×2 contingency table analysis comparing adhesions/no adhesions for old vs young gave a chi-squared value of 883.3, df=1, $p<0.0001$. Two-factor repeated measures indicated a significant interaction between age and # of adhesions: $F(4,196)=338.1$, $p<0.0001$. Planned contrasts post-anova show significant ($p<0.0001$) differences between old and young for each level of adhesion count (0, 1, 2, 3, and 4).

Results

AFM image and VSMC topography

Figure 1 displays contact mode height and surface map images of a typical VSMC isolated from an old and a young monkey. From this topological image data the cell area of old vs. young cells was 10,396±36 μm^2 vs. 10,150±48 μm^2 and the cell height of old vs. young cells was 3,370±247 nm vs. 2,936±203 nm. The images show the parallel banding of cortical actin fibers in the cells. From the images it is apparent that the actin filaments are more densely distributed in the old monkey VSMC compared to the young monkey VSMC. This is consistent with our previously published study in which we observed with immunofluorescent labeling and western blotting that old monkey cells expressed significantly more alpha-smooth muscle actin than young monkey cells (6). For all AFM experiments designed to evaluate elasticity and adhesion a measurement site was selected mid-way between the cell margin and the nucleus.

Real time elasticity measurements in single VSMC measured by AFM

For all cells studied the averaged elastic modulus was significantly higher ($P<0.001$) in VSMCs from old (22±2.9 kPa) compared to young (3.5±0.5 kPa) monkeys. The observation of a denser actin distribution and previously observed higher alpha smooth muscle actin expression (6) correlates with the higher measured elastic modulus in the older monkey VSMC compared to the younger monkey VSMC. Continuous measurements of the elasticity in single VSMC for a 30 min period indicated that elasticity exhibited temporal variations in both the old and young monkey VSMC (Figure 2A and B; blue trace). Comparison of the slope of the elasticity measurements (linear trend over time) indicated that the slope was not significantly different from 0 and that there was no difference between the old and young monkey VSMC (Table 1). Thus, the cells were stable during the 30 min measurement period and the indentation protocol for elasticity measurement was not having a cumulative effect on elasticity (repeated testing effect). A spectral analysis, based on signal strength, of the time varying behavior of the elasticity based on Eigen decomposition partitions was then undertaken. This permitted the amplitude, frequency and phase components of the oscillation pattern to be separated. Individual signals reconstructed from these components closely followed the principal oscillation patterns in the data for each cell (Figure 2A and B; red trace). To examine and compare the averaged group behavior of the oscillations, the three values of amplitude, frequency and phase for every experimental cell were averaged and then plotted (Figure 2C). A comparison of the averaged oscillation patterns in the old

and young monkey VSMC revealed significant differences between the two groups in terms of frequency and amplitude (Figure 2C). A more detailed analysis of the oscillation pattern over the 30 min period was performed to further characterize the three individual signal components that were identified in the elasticity measurements. These three components were individually 'stripped-out' to allow their separate characteristics to be examined (Figure 3; Table 1). For both the old and the young VSMC, the frequency and amplitudes were indirectly related to each other such that slowest component frequency had the highest component amplitude (Table 1). These spectral components were standardized and the individual frequency components plotted with the composite elasticity data for the VSMC old and young monkey groups (Figure 3). The first frequency component (large visible oscillation) was significantly faster in the old cells as compared to the young cells whereas there were no significant differences in frequency for the faster components 2 and 3 between the two groups (Figure 3; Table 1). The amplitudes of each of the three frequency components were significantly greater in old compared to young VSMCs (Table 1).

Real time measurement of ECM protein-integrin adhesion by AFM

We continuously measured, over a 30 min period, the adhesion to the ECM protein fibronectin (FN) and to a beta 1 integrin antibody and found that the adhesion was enhanced in VSMC from old (Figure 4) vs. young monkey (Figure 5) VSMC. The enhanced adhesion was observed for both the FN coated AFM probes and the beta 1 integrin antibody coated probes. There was no statistical difference in the adhesion to FN or the beta 1 integrin antibody in terms of recorded rupture forces and probability of binding. Consequently, these data sets were combined for an overall analysis of adhesive behavior. The enhanced adhesion was apparent as an increased unbinding force in old (85.8±5.6 pN) vs. young (43.0 ± 3.2 pN) and as an increased binding probability in old vs. young (Figure 5A; 5B; 5C; Table 1). The continuous real-time measurement of adhesion revealed that adhesion force like elasticity was oscillating with respect to time and also showed three major spectral components (Figures 4). In old monkey VSMC the oscillation occurred around a higher unbinding force and the amplitude of the oscillations in force were greater ($p<0.05$) than that observed in the younger monkey VSMC (Figure 5C; Table 1). The frequency of oscillation for component 1 was faster in the old monkey compared to the young but the frequencies of oscillation for the other components were not different between the young and the old VSMC (Figure 5C; Table 1). Comparison of the oscillation pattern observed in the recordings of unbinding force with those of cell elasticity revealed that the frequency of the force oscillations was significantly different for the slowest oscillation component for both the old and the young VSMC (Figure 4 and 5C; Table 1). The second and third spectral components of oscillation in unbinding force were not different from the frequencies observed in the cell elasticity (Figure 4 and 5C; Table 1). Furthermore, the oscillation pattern observed for the second and third oscillation component appear to be in phase and correlate with the oscillation of the second and third oscillation components observed in the cell elasticity (Figure 4 and 5C; Table 1) suggesting a mechanistic link between these two variables.

Effects of Cytochalasin D, ML7 or Blebbistatin on Elasticity

The involvement of the acin cytoskeleton as a determinant of VSMC elasticity was investigated by treating cells from old and young monkeys with an actin depolymerizing agent (cytochalasin D), a myosin light chain kinase inhibitor (ML7) or a myosin II inhibitor (blebbistatin) (Figures 6 and 7; Table 2: Figures S1-S3). In these experiments, a significant reduction in VSMC stiffness was observed following disruption of the actin cytoskeleton (old ~95%, young ~83%), inhibition of MLCK (old ~92%, young ~94%) or inhibition of myosin II (old ~37%, young ~80%) in cells from both old and young monkeys (Figures 7-8; Table 2). In addition, each of the treatments also significantly reduced the amplitude of all

three components of the detected oscillations (Figures 6 and 7; Table 2). Effects on the frequency of the oscillations were more variable. Cytochalasin D increased the frequency of components 2 and 3 in old but not young VSMC (Table 2), ML7 had no effects on oscillation frequencies in the old or young VSMC and blebbistatin slowed the frequency of component 1 in the young but not the old monkey VSMC (Table 2).

Discussion

We have developed a new strategy for analysis of dynamic time dependent changes in biomechanical behavior of cells using AFM to demonstrate that complex differences in the mechanical properties of VSMC occur in aging. Real-time elasticity and adhesion measurements were made in single aortic vascular smooth muscle cells (VSMC) from old and young male monkeys (Macaca fascicularis) using a force-indentation method with AFM. A spectral analysis of the results clearly demonstrated the presence of dynamic oscillatory behavior in cell elasticity that is driven by actinmyosin interactions. The analysis further revealed oscillation patterns in cellular adhesion to the extracellular matrix (ECM) protein, fibronectin (FN) that were highly synchronized with the oscillations in cell elasticity. Oscillatory patterns exhibited for both elasticity and adhesion were different between the old and the young monkeys. These observations significantly extend previous findings (6) that VSMC from old monkeys had a higher average elastic modulus compared to young monkeys and they provide direct biomechanical evidence for age-induced alterations in the biochemical processes that regulate cytoskeletal and adhesive behavior. The observation that the elastic modulus and adhesion of VSMC is elevated in aging is physiologically relevant as it points to the possibility that dynamic, time-dependent factors may contribute to the increased vascular stiffness that accompanies aging.

In a previous study we reported that aortic VSMC from old monkeys had a significantly higher average elastic modulus than cells for younger monkeys (6). It was concluded that the increase in stiffness was related to an increased expression of smooth muscle alpha actin. In the this study we have extended these observations, to show that the VSMC elasticity is exhibiting oscillations and that the differences in stiffness and the oscillations were largely eliminated by treatment of the cells with the actin depolymerizing agent, cytochalasin D, by treatment with the myosin light chain kinase inhibitor, ML7 and by treatment with the myosin II inhibitor, blebbistatin. These observations strongly support a functional as well as a structural role for actin and myosin in altering cellular mechanical properties during aging.

The observation that elasticity exhibits strong oscillatory behavior suggest that the moment to moment dynamic behavior of the cytoskeleton needs to be more closely examined as a contributing factor underlying altered aortic stiffness in aging. Although, the mechanisms driving this periodic behavior were not part of this study, the ability to carefully analyze and quantify the oscillatory behavior provides a basis for further mechanistic investigations. Based on our observations it is reasonable to speculate about some likely possibilities. Since we have shown that the elasticity and oscillations involve the actin cytoskeleton in this VSMC model, an oscillation in cross-bridge cycling could be driven by oscillations related to Ca^{2+} signaling (7, 34-43) and/or oscillations in signaling that governs myosin light chain phosphorylation (34,35). Likewise, oscillation in pathways regulating polymerization and depolymerization of the actin cytoskeleton could also be involved (34). The observation that there were three different spectral components identified in the oscillation pattern make it reasonable to hypothesize that more than one mechanism is contributing to the spontaneous oscillations in cell elasticity and thus could play a role in the enhanced vascular stiffness observed in aging.

Recently, Schillers et al. (28) used a very similar AFM protocol for real-time measurement of cell elasticity in bronchial epithelial cells. They also observed that cell elasticity exhibited spontaneous and periodic oscillations (200 s period and ~0.15 kPa amplitude) that were inhibited by an actin depolymerization agent (latrunculin A), by depletion of $Ca^{2+}$with a Ca^{2+} chelating agent (BAPTA-AM) and by a myosin II inhibitor (blebbistatin). Oscillations were also enhanced by a Ca^{2+} ionophore (ionomycin) and by a Ca^{2+}-ATPase inhibitor (thapsigargin). Thus, these observations, combined with those in the present study, support the idea that time-dependent oscillations in cell elasticity are a normal characteristic of a dynamic cytoskeletal system and that they are strongly influenced by actin cytoskeletal dynamics. Their analytical approach included a smoothing routine that eliminated higher frequency oscillation components so it is not possible to quantify frequency and amplitude of higher order components if they were present. None-the-less, Schillers et al. (28) observations and ours indicate that dynamic mechanical oscillations are a fundamental property of living cells.

As we have previously reported (6), adhesion to FN was enhanced in the VSMC from old monkeys compared to young monkeys. This was apparent as a rightward shift in the histogram display of unbinding forces and as an increased probability of binding. We previously reported that this enhanced adhesion to FN in old monkeys was correlated with an enhanced expression of beta 1 integrin (6). In the present study, adhesion was assessed continuously over time by using AFM probes that were functionalized with FN to allow adhesion to be correlated with elasticity. Similar to VSMC elasticity, the adhesion was found to oscillate with time and three major spectral components of oscillation were detected. Comparisons of the oscillation pattern for adhesion between the old monkey and young monkey VSMC revealed that although the frequencies of the separate oscillation components were similar, the amplitudes were significantly greater for all three oscillatory components in old monkey cells compared to young monkey VSMC. When the oscillation pattern seen in adhesion was compared to the pattern for elasticity, it was found that the slowest component of oscillatory behavior in adhesion (component 1) was faster than the slowest oscillation wave in elasticity (component 1). In contrast, adhesion components 2 and 3 correlated well with the pattern of change observed in components 2 and 3 in the elasticity waveform. This was true for both the old and young monkey VSMC. These oscillating biomechanical events are very likely manifestations of oscillations in biochemical signaling events taking place in the VSMC. Given this interpretation, the lack of correlation in frequency between elasticity and adhesion for the slow wave (component 1) suggests that the signaling mechanisms driving this oscillatory component are different for these two biomechanical phenomena. Likewise, the similarities in the frequency in oscillation in elasticity and adhesion for components 2 and 3 are interpreted to indicate that the underlying signaling mechanism is shared. In this case, the oscillating biochemical events are interacting in an inside-out manner with integrin signaling pathways.

Interplay occurring between mechanical force and focal adhesion events has been previously demonstrated (26,27,44). In our cell system the mechanical forces are being generated by internal cellular processes as opposed to outside-in transmission of forces from the ECM. It is of interest that the adhesion changes we are observing reflect cycling in integrin adhesiveness for non-force bearing sites on the cell surface. Thus, as the cell elastic modulus increases it appears to occur in tandem with activation of adhesion mechanisms. One possibility is that the activation of the integrin adhesion is being mediated by an increase in intracellular force within the cell and that this is mechanically activating the integrin (6,27). A second possibility is that the activation is occurring through a cytoplasmic signaling molecule. In either case, a link would be provided that integrates internal mechanical force/force generation with the integrin receptor signaling state. The correlation between the elasticity and the adhesion has significant implications for a force-generating cell like a

VSMC. The coordination of elasticity/cytoskeletal change with adhesion provides a mechanism that could strengthen attachment sites and stabilize cytoskeletal anchoring when VSMC are activated (i.e. contracting/stiffening) and likewise relax attachment when cytoskeletal tension decreases. Another functional implication is that the cycling of the integrin activation could play a role in allowing the cell to sense its surrounding environment and search for ECM protein binding sites. In spreading fibroblast cells activated beta 1 integrins driven by actin are found at the leading edge of the cell and appear to behave like “sticky fingers” searching for an ECM binding sites (45). If they bind and form a new or nascent adhesion then exposure of the site to force may be important in triggering whether they go through a process of maturation to fully develop into focal adhesions.

Oscillations represent an intrinsic property of biological systems and cells (16). They are the result of the complex biophysical and biochemical interactions that take place within the cell. One important source of cellular oscillations involves cytoskeletal structures that are responsible for cellular mobility and generation of force (16,17,18,19). The functional purpose of an oscillation in elasticity is not clearly known. Several possibilities exist including the possibility that the cell is actively sensing the mechanical characteristics of its environment. Another possibility is that it could be a means for biomechanically signaling neighboring cells. As pointed out by Schillers (28) it would be of interest to know whether the oscillation pattern in a community of connected cells is coordinated in a synchronous fashion. In our study and in the study reported by Schillers et al. (28) the AFM can only assess one site on the cell at a time. Thus, other questions that remain to be addressed include to what extent does the localized activity represent the global biomechanical activity of the cell. To examine this question in more detail we also analyzed the contact point or z-axis position of the AFM probe when it contacted the cell membrane and first encountered resistance sufficient to induce deflection of the probe. We found that the contact point oscillated with the same pattern (data not shown) as the elasticity indicating that the three major oscillatory components we analyzed were reflected in changes in whole cell height. We interpret this to indicate that the oscillation pattern we studied reflected whole cell behavior and a localized event. Future studies to address this question will require use of force measuring techniques to enable detection and measurement of changes in nano-scale forces at multiple sites simultaneously and across multiple cells that are interconnected. Such behavior indicates that the cells may well be continuously adjusting their internal mechanical and adhesive state.

In our studies, the use of the time resolved analytical approach to understand the real-time mechanical and adhesive behavior of cells provides a unique opportunity to detect and analyze functional differences between cells and provides a useful tool for diagnostic characterization of cells. Using this approach, we have determined that VSMC from old monkeys had increased elasticity and enhanced adhesion to FN compared to young. Both elasticity and adhesion displayed oscillatory components during real time recording of these variables and the waveforms differed between old and young monkeys. These observations suggest that cellular mechanisms regulating cell elasticity and adhesion are affected differently during aging and that they are interlinked. These differences may play an important role in the vascular remodeling changes that lead to stiffening of the vascular wall with aging. For example, VSMC that are stiffer and display pronounced oscillations in elasticity with enhanced adhesion to the ECM could actively enhance vascular stiffness by increasing the active stress within the vascular wall. It is conceivable that strategies for treatment of vascular stiffness could be developed with targeting of these dynamic elements and/or their coupling in mind. The ability to biomechanically convert an old cell to a phenotype resembling a young cell would be a very relevant goal and represent and exciting new approach to consider for treatment of the stiffening that occurs with aging. Certainly an

important next step will be to correlate these mechanical measures with biochemical and molecular measures to further improve our ability to resolve questions concerning the signaling that is controlling the oscillation and the coupling of cell elasticity and adhesion.

Supplementary Material

Refer to Web version on PubMed Central for supplementary material.

Acknowledgments

Funding Support This work supported, in part, by NIH grants HL1024720, AG027211, HL033107, HL069752, HL095888, HL069020, HL58960, HL062863, AG023567 and P01 HL095486

References

1. Intengan HD, Schiffrin EL. Structure and mechanical properties of resistance arteries in hypertension: role of adhesion molecules and extracellular matrix determinants. Hypertension. 2000; 36(3):312–8. [PubMed: 10988257]
2. Lakatta EG. Age-associated cardiovascular changes in health: impact on cardiovascular disease in older persons. Heart Fail Rev. 2002; 7(1):29–49. [PubMed: 11790921]
3. Lakatta EG, Sollott SJ. Perspectives on mammalian cardiovascular aging: humans to molecules. Comp Biochem Physiol A Mol Integr Physiol. 2002; 132(4):699–721. [PubMed: 12095857]
4. Lacolley P, et al. Prevention of aortic and cardiac fibrosis by spironolactone in old normotensive rats. J Am Coll Cardiol. 2001; 37(2):662–7. [PubMed: 11216994]
5. Qiu H, et al. Mechanism of gender-specific differences in aortic stiffness with aging in nonhuman primates. Circulation. 2007; 116(6):669–76. [PubMed: 17664374]
6. Qiu H, et al. Short communication: vascular smooth muscle cell stiffness as a mechanism for increased aortic stiffness with aging. Circ Res. 2010; 107(5):615–9. [PubMed: 20634486]
7. Gerthoffer WT. Actin cytoskeletal dynamics in smooth muscle contraction. Can J Physiol Pharmacol. 2005; 83(10):851–6. [PubMed: 16333356]
8. Vats P, et al. The dynamic nature of the bacterial cytoskeleton. Cell Mol Life Sci. 2009; 66(20): 3353–62. [PubMed: 19641848]
9. Hinz B, Gabbiani G. Mechanisms of force generation and transmission by myofibroblasts. Curr Opin Biotechnol. 2003; 14(5):538–46. [PubMed: 14580586]
10. Mitchell GF, et al. Cross-sectional correlates of increased aortic stiffness in the community: the Framingham Heart Study. Circulation. 2007; 115(20):2628–36. [PubMed: 17485578]
11. Berrier AL, Yamada KM. Cell-matrix adhesion. J Cell Physiol. 2007; 213(3):565–73. [PubMed: 17680633]
12. Levental KR, et al. Matrix crosslinking forces tumor progression by enhancing integrin signaling. Cell. 2009; 139(5):891–906. [PubMed: 19931152]
13. Schwartz MA, Ginsberg MH. Networks and crosstalk: integrin signalling spreads. Nat Cell Biol. 2002; 4(4):E65–8. [PubMed: 11944032]
14. Galbraith CG, et al. The relationship between force and focal complex development. J Cell Biol. 2002; 159(4):695–705. [PubMed: 12446745]
15. Parsons JT, et al. Cell adhesion: integrating cytoskeletal dynamics and cellular tension. Nat Rev Mol Cell Biol. 2010; 11(9):633–43. [PubMed: 20729930]
16. Kruse K, Julicher F. Oscillations in cell biology. Curr Opin Cell Biol. 2005; 17(1):20–6. [PubMed: 15661515]
17. Placais PY, et al. Spontaneous oscillations of a minimal actomyosin system under elastic loading. Phys Rev Lett. 2009; 103(15):158102. [PubMed: 19905668]
18. Ishiwata S, et al. Contractile system of muscle as an auto-oscillator. Prog Biophys Mol Biol. 2011; 105(3):187–98. [PubMed: 21163290]

19. Ishiwata S, et al. Molecular motors as an auto-oscillator. HFSP J. 2010; 4(3-4):100–4. [PubMed: 21119762]
20. Radmacher M. Studying the mechanics of cellular processes by atomic force microscopy. Methods Cell Biol. 2007; 83:347–72. [PubMed: 17613316]
21. Hemmer JD, et al. Role of cytoskeletal components in stress-relaxation behavior of adherent vascular smooth muscle cells. J Biomech Eng. 2009; 131(4):041001. [PubMed: 19275430]
22. Labernadie A, et al. Dynamics of podosome stiffness revealed by atomic force microscopy. Proc Natl Acad Sci U S A. 2010; 107(49):21016–21. [PubMed: 21081699]
23. Mathur AB, et al. Endothelial, cardiac muscle and skeletal muscle exhibit different viscous and elastic properties as determined by atomic force microscopy. J Biomech. 2001; 34(12):1545–53. [PubMed: 11716856]
24. Watanabe-Nakayama T, et al. Direct detection of cellular adaptation to local cyclic stretching at the single cell level by atomic force microscopy. Biophys J. 2011; 100(3):564–72. [PubMed: 21281570]
25. Sun Z, et al. Probing cell surface interactions using atomic force microscope cantilevers functionalized for quantum dot-enabled Forster resonance energy transfer. J Biomed Opt. 2009; 14(4):040502. [PubMed: 19725707]
26. Sun Z, et al. Extracellular matrix-specific focal adhesions in vascular smooth muscle produce mechanically active adhesion sites. Am J Physiol Cell Physiol. 2008; 295(1):C268–78. [PubMed: 18495809]
27. Sun Z, et al. Mechanical properties of the interaction between fibronectin and alpha5beta1-integrin on vascular smooth muscle cells studied using atomic force microscopy. Am J Physiol Heart Circ Physiol. 2005; 289(6):H2526–35. [PubMed: 16100245]
28. Schillers H, et al. Real-time monitoring of cell elasticity reveals oscillating myosin activity. Biophys J. 2010; 99(11):3639–46. [PubMed: 21112288]
29. Vegh AG, et al. Spatial and temporal dependence of the cerebral endothelial cells elasticity. J Mol Recognit. 2011; 24(3):422–8. [PubMed: 21504019]
30. Schaffner-Reckinger E, et al. Distinct involvement of beta3 integrin cytoplasmic domain tyrosine residues 747 and 759 in integrin-mediated cytoskeletal assembly and phosphotyrosine signaling. J Biol Chem. 1998; 273(20):12623–32. [PubMed: 9575224]
31. Crick SL, Yin FC. Assessing micromechanical properties of cells with atomic force microscopy: importance of the contact point. Biomech Model Mechanobiol. 2007; 6(3):199–210. [PubMed: 16775736]
32. Hassani H. Singular spectrum analysis: methodology and comparison. Journal of Data Science. 2007; 5:239–57.
33. Elsner, JBT.; A.A.. Singular Spectrum Analysis: A new tool in time series analysis. Plenum Press; New York: 1996. p. 45
34. Kim TJ, et al. Substrate rigidity regulates Ca2+ oscillation via RhoA pathway in stem cells. J Cell Physiol. 2009; 218(2):285–93. [PubMed: 18844232]
35. Tsien RW, Tsien RY. Calcium channels, stores, and oscillations. Annu Rev Cell Biol. 1990; 6:715–60. [PubMed: 2177344]
36. Kummer U, et al. Switching from simple to complex oscillations in calcium signaling. Biophys J. 2000; 79(3):1188–95. [PubMed: 10968983]
37. Gerthoffer WT. Signal-transduction pathways that regulate visceral smooth muscle function. III. Coupling of muscarinic receptors to signaling kinases and effector proteins in gastrointestinal smooth muscles. Am J Physiol Gastrointest Liver Physiol. 2005; 288(5):G849–53. [PubMed: 15826932]
38. Haddock RE, Hill CE. Rhythmicity in arterial smooth muscle. J Physiol. 2005; 566(Pt 3):645–56. [PubMed: 15905215]
39. Imtiaz MS, et al. Synchronization of Ca2+ oscillations: a coupled oscillator-based mechanism in smooth muscle. FEBS J. 2010; 277(2):278–85. [PubMed: 19895582]
40. Lee CH, et al. Asynchronous calcium waves in smooth muscle cells. Can J Physiol Pharmacol. 2005; 83(8-9):733–41. [PubMed: 16333375]

41. Kuo KH, et al. Relationship between asynchronous Ca2+ waves and force development in intact smooth muscle bundles of the porcine trachea. Am J Physiol Lung Cell Mol Physiol. 2003; 285(6):L1345–53. [PubMed: 12936908]

42. Perez JF, Sanderson MJ. The contraction of smooth muscle cells of intrapulmonary arterioles is determined by the frequency of Ca2+ oscillations induced by 5-HT and KCl. J Gen Physiol. 2005; 125(6):555–67. [PubMed: 15928402]

43. Uhlen P, Fritz N. Biochemistry of calcium oscillations. Biochem Biophys Res Commun. 2010; 396(1):28–32. [PubMed: 20494106]

44. Na S, et al. Time-dependent changes in smooth muscle cell stiffness and focal adhesion area in response to cyclic equibiaxial stretch. Ann Biomed Eng. 2008; 36(3):369–80. [PubMed: 18214679]

45. Galbraith CG, et al. Polymerizing actin fibers position integrins primed to probe for adhesion sites. Science. 2007; 315(5814):992–5. [PubMed: 17303755]

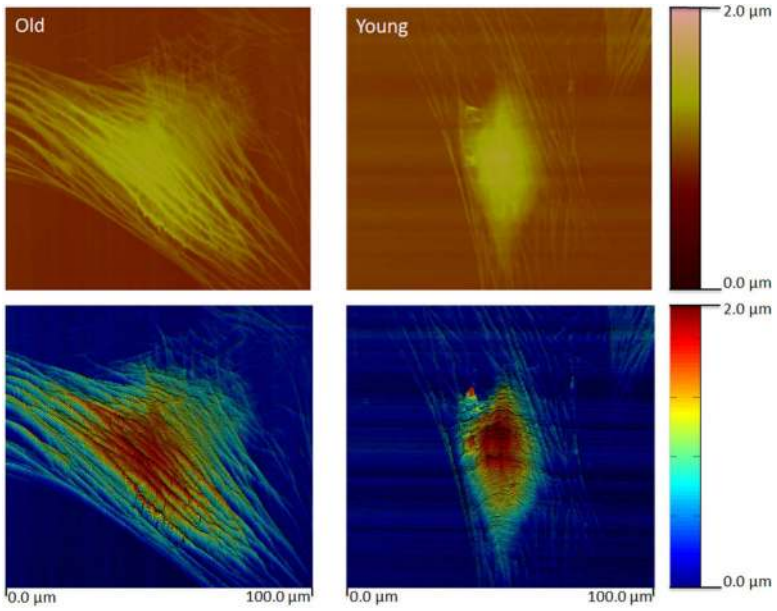

Figure 1.
Examples of a contact mode height image (top) and a surface plot image are shown for a typical old and young monkey aortic VSMC. The height image data was fitted with a surface, pseudo-colored and slightly tilted to enhance relief contrast. The images reveal a more extensive network of cortical actin filaments in the old monkey VSMC compared to the Young monkey VSMC. The color bars at the right of the image index the cell height. A size scale is shown at the bottom of the images.

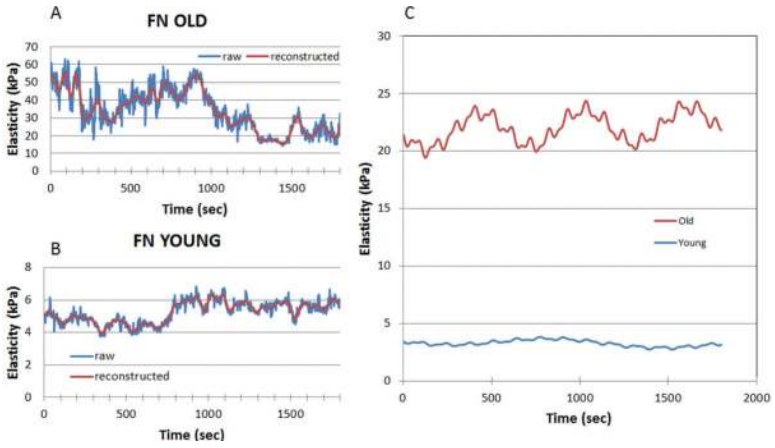

Figure 2.

An example is shown of a 30 min recording of cell elastic modulus for a typical old (A) and young (B) monkey VSMC. The blue line displays the raw data collected and the red line displays the reconstructed data after processing. Processing of the data involved eigen decomposition partitions based on signal strength to permit the amplitude, frequency and phase components of the oscillation to be separated. Composite data for the group of old VSMC (n=24) and young (n=27) show pronounced differences in oscillatory behavior of old and young VSMC as well as reveal several different oscillatory components underlying the dynamic changes in cell elastic modulus in each group (C).

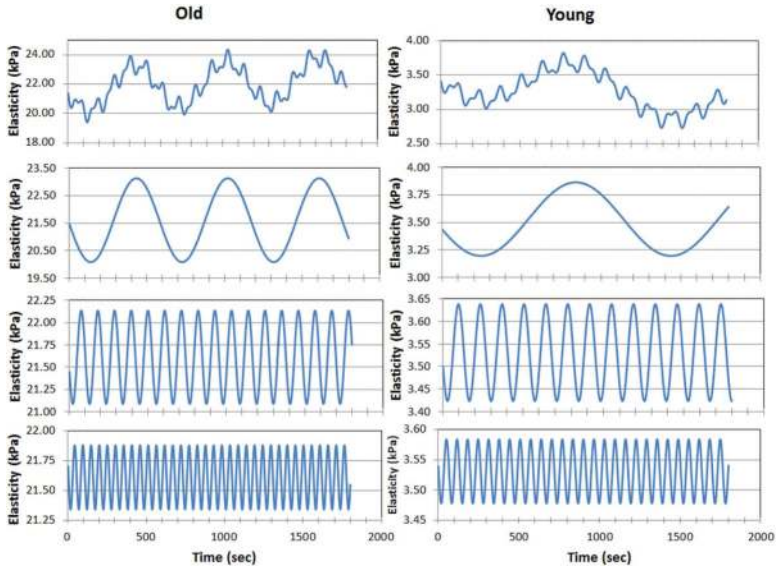

Figure 3.

Mathematical decomposition of the elastic modulus waveform for each group revealed three principle components of oscillation. The top panels show the oscillations plotted as elastic modulus in composite waveform format for the old and young monkey VSMC. The three panels beneath the composite plot show, from slowest to fastest, the three detected oscillatory components. Frequency, amplitude and phase are given in Table 1.

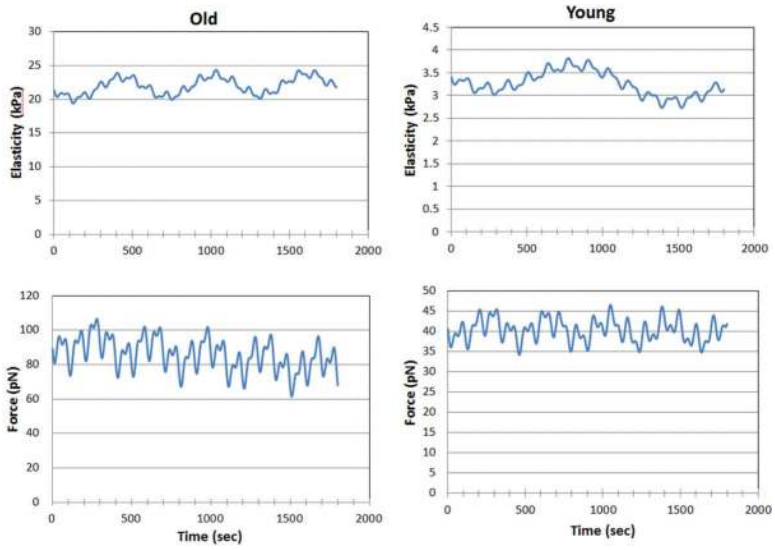

Figure 4.

Comparison of the oscillation patterns for VSMC elastic modulus and unbinding force representing adhesion to AFM probes coated with FN or a beta 1 integrin antibody for old (right panels) and young (left panels) monkey VSMC. A difference in the oscillation frequency for component 1, slowest visible component, is apparent between elasticity and unbinding force whereas the oscillation frequencies for components 2 and 3 are not different between elastic modulus and unbinding force. Data are plotted in units of kPa for elastic modulus and pN for unbinding force.

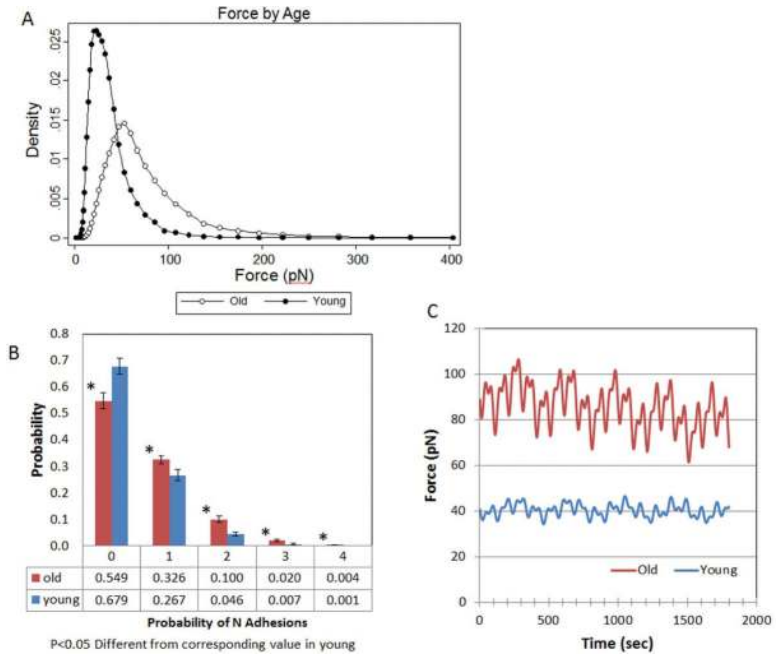

	0	1	2	3	4
old	0.549	0.326	0.100	0.020	0.004
young	0.679	0.267	0.046	0.007	0.001

Figure 5.

Unbinding forces for old and young monkey VSMC are shown in this figure. Panel A displays overlay plots of the force-adhesion events distributions plotted as histograms. The plot shows the probability density distribution of force and illustrates the higher peak binding forces observed in the old monkey VSMC. Panel B displays the observed probabilities calculated from the AFM retraction curves that record adhesion events. In total, 22988 retraction curves were obtained from old monkeys (958 ± 32 curves/cell); 23771 curves were obtained from young monkeys (880 ± 50 curves/cell). In this bar graph, the probability of observing 0, 1, 2, 3 or 4 adhesion events in an experimentally obtained retraction curve is plotted. Standard error bars indicate the between monkey variability. Asterisks indicate significant differences between the old and young monkey VSMC. These data show a higher probability of 0 events in the young monkey VSMC but a lower probability of multiple adhesion events per sampled retraction curve. These observations indicate that the old monkey VSMC were more adhesive than the young. Panel C shows a comparison of the real-time recordings of adhesion from the old and young monkey VSMC groups. The old monkey VSMC also displayed higher amplitude oscillations in the unbinding force.

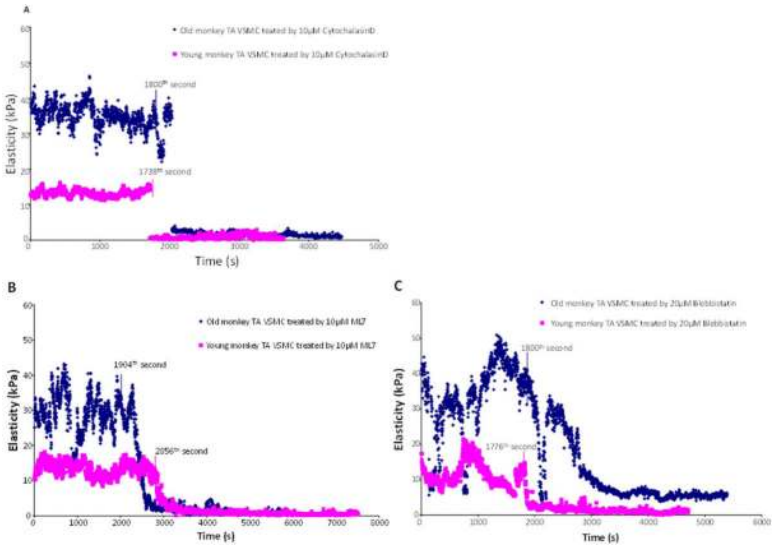

Figure 6.

Examples are shown of ~30 min recordings of real-time cell elastic modulus for typical old (blue diamonds) and young (purple squares) monkey VSMC. Panels A, B and C show cell responses from experiments using cytochalasin D, ML7 or blebbistatin, respectively. Drug additions are shown with time marking the time of addition in seconds.

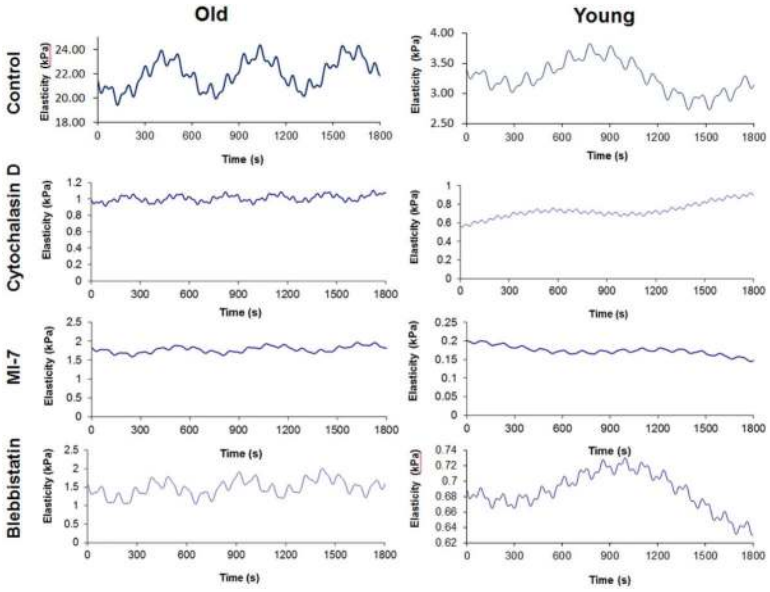

Figure 7.

Comparison of the oscillation patterns for VSMC elastic modulus for the old and young monkey VSMC groups shown in top panels. Panels below show composite group data for post-drug treated cells for cytochalasin D, ML7 and blebbistatin, respectively. The data show the significant reduction in elasticity and oscillation amplitude following drug treatments.

Table 1

Mean and SEM for the oscillatory components of elasticity and adhesion forces for old and young monkey VSMC.

		Elasticity (kPa)		Force (pN)	
Component	**Parameter**	**Old (n=24)**	**Young (n=27)**	**Old (n=24)**	**Young (n=27)**
1	Frequency (Hz)	$1.70\ (0.41) \times 10^{-3}$ *b*	$8.38\ (3.91) \times 10^{-4}$	$3.03\ (0.37) \times 10^{-3}$ *b*	$2.37\ (0.38) \times 10^{-3}$
2	Frequency (Hz)	$9.40\ (1.07) \times 10^{-3}$	$7.34\ (0.58) \times 10^{-3}$	$1.05\ (0.08) \times 10^{-2}$	$9.39\ (0.67) \times 10^{-3}$
3	Frequency (Hz)	$1.92\ (0.24) \times 10^{-2}$	$1.53\ (0.12) \times 10^{-2}$	$2.01\ (0.13) \times 10^{-2}$	$1.78\ (0.12) \times 10^{-2}$
1	Amplitude[a]	1.52 (0.53) *b*	0.334 (0.097)	5.36 (0.94) *b*	2.86 (0.74)
2	Amplitude[a]	0.523 (0.153) *b*	0.107 (0.021)	6.4 (1.1) *b*	2.64 (0.47)
3	Amplitude[a]	0.270 (0.076) *b*	0.052 (0.015)	4.4 (1.0) *b*	1.95 (0.29)
1	Phase (sec)	3.23 (0.36)	3.42 (0.32)	3.40 (0.36)	3.27 (0.29)
2	Phase (sec)	3.35 (0.43)	3.35 (0.35)	3.41 (0.33)	2.97 (0.37)
3	Phase (sec)	2.54 (0.36)	2.79 (0.34)	3.49 (0.33)	3.36 (0.35)
---	Intercept[a]	21.6 (2.9) *b*	3.53 (0.47)	85.8 (5.6) *b*	43.0 (3.2)
---	Slope	$4.4\ (26.5) \times 10^{-4}$	$2.27\ (4.15) \times 10^{-4}$	$-7.56\ (3.39) \times 10^{-3}$	$1.8\ (11.3) \times 10^{-4}$

[a] Values are expressed in the same units as the parent measure (kPa for elasticity and pN for force)

[b] Different from corresponding value in young subjects, $p < 0.05$

Aging Cell. Author manuscript; available in PMC 2013 October 01.

Table 2

Mean and SEM of oscillatory components of cell elasticity following treatment with cytochalasin D, ML7 or blebbistatin for old and young monkey VSMC.

		Cytochalasin D		ML-7		Blebbistatin	
Component	**Parameter**	**Old (n=5)**	**Young (n=5)**	**Old (n=5)**	**Young (n=4)**	**Old (n=12)**	**Young (n=11)**
1	Frequency (Hz)	$3.30\ (2.07) \times 10^{-3}$	$7.84\ (7.60) \times 10^{-4}$	$1.76\ (4.00) \times 10^{-3}$	$7.60\ (8.19) \times 10^{-4}$	$2.04\ (0.99) \times 10^{-3}$ *a*	$6.14\ (1.66) \times 10^{-4}$ *b*
2	Frequency (Hz)	$1.44\ (0.50) \times 10^{-2}$ *b*	$8.35\ (5.38) \times 10^{-3}$	$9.12\ (3.86) \times 10^{-3}$	$8.03\ (23.9) \times 10^{-3}$	$9.67\ (1.47) \times 10^{-3}$	$7.81\ (2.0) \times 10^{-3}$
3	Frequency (Hz)	$2.66\ (1.12) \times 10^{-2}$ *b*	$2.06\ (6.63) \times 10^{-2}$	$1.79\ (7.06) \times 10^{-2}$	$1.9\ (14.3) \times 10^{-2}$	$2.04\ (0.44) \times 10^{-2}$	$2.08\ (0.48) \times 10^{-2}$
1	Amplitude (kPa)	$4.41\ (5.60) \times 10^{-2}$ *b*	$5.7\ (13.6) \times 10^{-2}$	$9.27\ (6.01) \times 10^{-2}$ *ab*	$9.3\ (25.5) \times 10^{-3}$ *b*	$0.228\ (0.114)$ *ab*	$3.28\ (1.48) \times 10^{-2}$ *b*
2	Amplitude (kPa)	$2.14\ (0.66) \times 10^{-2}$ *b*	$1.01\ (0.47) \times 10^{-2}$ *b*	$4.41\ (5.60) \times 10^{-2}$ *ab*	$4.48\ (3.21) \times 10^{-3}$ *b*	$0.160\ (0.088)$ *ab*	$7.34\ (3.63) \times 10^{-3}$ *b*
3	Amplitude (kPa)	$1.43\ (1.59) \times 10^{-2}$ *b*	$1.51\ (0.32) \times 10^{-2}$ *b*	$1.55\ (2.95) \times 10^{-2}$ *ab*	$8.50\ (7.95) \times 10^{-4}$ *b*	$4.85\ (2.19) \times 10^{-2}$ *ab*	$3.79\ (1.41) \times 10^{-3}$ *b*
1	Phase (sec)	3.19 (1.33)	5.48 (1.93)	2.05 (0.52)	1.74 (1.58)	2.16 (0.57)	3.90 (0.83)
2	Phase (sec)	2.88 (1.87)	2.56 (0.31)	2.88 (1.15) *b*	2.69 (0.72)	2.77 (0.43)	3.32 (0.63)
3	Phase (sec)	2.99 (0.36)	3.55 (0.49)	1.81 (1.16)	5.40 (2.39)	2.67 (0.67)	2.67 (0.66)
---	Intercept (kPa)	0.987 (6.339) *b*	0.608 (0.563) *b*	1.73 (4.68) *b*	0.191 (0.440) *b*	1.97 (2.53) *b*	0.712 (0.315) *b*
---	Slope (kPa/sec)	$2.65\ (2.41) \times 10^{-4}$	$1.33\ (7.21) \times 10^{-4}$	$6.1\ (26.3) \times 10^{-5}$	$1.9\ (27.4) \times 10^{-5}$	$1.89(2.0) \times 10^{-4}$ *b*	$-2.50(8.71) \times 10^{-5}$ *b*

a Different from corresponding value in young subjects, $p < 0.05$

b Different from corresponding value in control (Pre-drug) period, $p < 0.05$